

The role of surface freshwater flux boundary conditions in Arctic Ocean modelling

M. Prange ^{a,*}, R. Gerdes ^b

^a *DFG Research Center Ocean Margins and Department of Geosciences, University of Bremen, D-28334 Bremen, Germany*

^b *Alfred Wegener Institute for Polar and Marine Research, D-27570 Bremerhaven, Germany*

Received 4 April 2005; received in revised form 27 September 2005; accepted 28 September 2005

Available online 24 October 2005

Abstract

The role of surface freshwater flux boundary conditions in prognostic Arctic Ocean/sea-ice modelling is analysed, using a regional numerical model. Three different applications of freshwater flux formulations are evaluated. The standard formulation, which serves as a benchmark, takes surface volume fluxes due to precipitation, evaporation and river runoff into account. The total freshwater input to the Arctic Ocean by runoff, precipitation and Bering Strait inflow is approximately $6800 \text{ km}^3 \text{ yr}^{-1}$ in the model setup. The implementation of an Arctic river water tracer in the standard run enables the calculation of an average mean residence time of 14–15 years for river water in the Arctic halocline. The second formulation for surface freshwater fluxes neglects the volume input, which corresponds to applying ‘virtual salinity fluxes’. This simplification leads to a rapid salinity build-up in the upper layers of the Arctic Ocean and causes a substantial reduction of freshwater export through Fram Strait. The third formulation uses a constant reference salinity of 35 psu in the definition of the virtual salinity flux boundary condition. This approach results in hydrographic fields which are very similar to those from the standard run. Errors in circulation and freshwater transport are small and, for most applications, tolerable. Our results suggest that virtual salinity fluxes with fixed reference salinity are a reasonable approximation for Arctic Ocean models with horizontal resolution of order 100 km.

© 2005 Elsevier Ltd. All rights reserved.

Keywords: Ocean/sea-ice modelling; Surface freshwater flux boundary conditions; Goldsbrough circulation; Arctic Ocean freshwater balance; River runoff

1. Introduction

Relative to its size, the Arctic Ocean (Fig. 1) receives the largest river water input of all oceans (Grabs et al., 1996). This freshwater supply is of paramount importance for density-driven dynamics and stratification in polar regions, since the density of near-freezing water is primarily a function of salinity (e.g., Semtner, 1984, 1987; Ranelli and Hibler, 1991; Holland et al., 1996; Zhang et al., 1998; Prange and Lohmann, 2003,

* Corresponding author. Tel.: +49 421 218 7187.

E-mail address: mprange@palmod.uni-bremen.de (M. Prange).

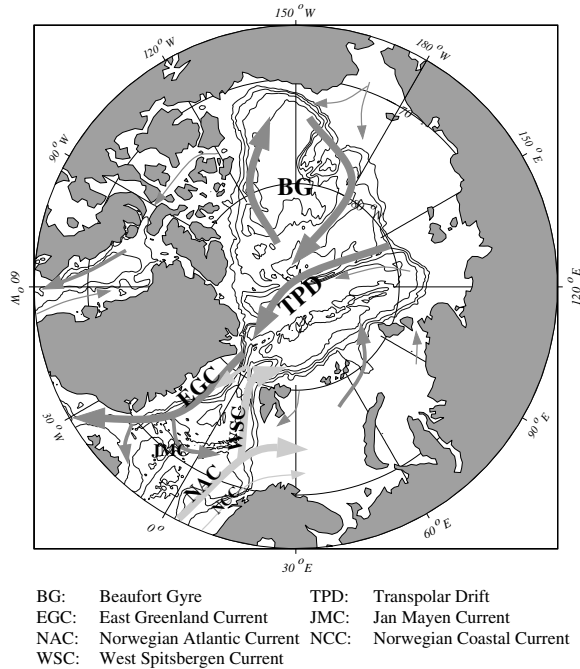


Fig. 1. Sketch of the mean surface circulation in the Arctic Mediterranean. Warm (cold) currents are displayed by light (dark) grey arrows.

2004). The freshwater surplus of the Arctic Ocean is balanced by freshwater exports—as liquid water and sea-ice—through Fram Strait and the Canadian Archipelago (Aagaard and Carmack, 1989). The largest term in the freshwater balance of the Arctic Ocean is river runoff. About $3 \times 10^3 \text{ km}^3 \text{ yr}^{-1}$ of river water flows into the Arctic Ocean (Aagaard and Carmack, 1989; Prowse and Flegg, 2000). More than 50% of this freshwater is provided by the four largest Arctic rivers, namely Yenisey, Lena, Ob, and Mackenzie. The freshwater supply to the Arctic Ocean is expected to increase in the future due to enhanced poleward moisture transports in a warmer atmosphere (e.g., Miller and Russell, 1995; Peterson et al., 2002), thawing of permafrost (Zhang et al., submitted for publication) and melting of the Greenland ice sheet (Gregory et al., 2004).

In spite of its importance, little attention has been paid to the freshwater budget in Arctic Ocean/sea-ice models. Most Arctic Ocean general circulation models (OGCMs) apply salinity restoring to climatological data in order to maintain a realistic hydrography (see Steiner et al. (2004) and references therein). Salinity restoring is introduced by an unphysical diagnostic term into the equations of an OGCM, which may dampen and distort ocean variability (Simmons and Polyakov, 2004). Moreover, restoring makes a model unsuitable for paleoceanographic applications where no observational data are available. In this paper, we concentrate on ‘prognostic’ modelling; that is, modelling of the general ocean/sea-ice circulation without introduction of any diagnostic restoring or nudging into the model equations. So far, only few OGCMs of the Arctic Ocean run in a prognostic mode by omitting salinity restoring (Häkkinen, 1999; Holloway and Sou, 2002). In these models, however, surface freshwater fluxes are treated in a simplified way using a ‘virtual salinity flux’ formulation (e.g., Huang, 1993; Barnier, 1998).

The basic assumption of the virtual salinity flux formulation is that vertical velocities due to precipitation P , evaporation E and river runoff R are negligible in the surface kinematic boundary condition (e.g., Roulet and Madec, 2000). In the discretized system of equations in a finite-difference OGCM, surface freshwater fluxes ($-P + E - R$) then only appear in the salinity equations of the topmost grid boxes as virtual salinity fluxes (e.g., Barnier, 1998)

$$F_S = (-P + E - R)S_1, \quad (1)$$

where S_1 denotes salinities of the surface boxes. The salinity flux boundary condition (1) introduces an undesirable positive feedback: In regions where the local surface salinity S_1 increases owing to excess evaporation, the surface salinity flux F_S increases proportional to S_1 . The enhanced salinity flux F_S leads to a further increase in S_1 , and so on. Due to the correlation between surface salinity and freshwater flux, the flux boundary condition (1) may result in a global salinity explosion even when the globally integrated $(-P + E - R)$ is zero (Huang, 1993; Roulet and Madec, 2000). In order to eliminate this feedback and the associated non-conservative nature of boundary condition (1), a globally constant reference salinity S_{ref} is often used in the formulation of the haline surface flux (cf. Pardaens et al., 2003):

$$F_S = (-P + E - R)S_{\text{ref}}. \quad (2)$$

Using boundary condition (2), the strength of the haline forcing depends on the choice of S_{ref} . It is important to note that condition (2) is only a reasonable approximation, if surface salinities are not too far from the reference salinity; that is, $S_1 \approx S_{\text{ref}}$.

Within the framework of the ‘Arctic Ocean Model Intercomparison Project’ (AOMIP) Steele et al. (2001a) found that current Arctic Ocean models have a bias towards overly salty surface conditions within the Beaufort Gyre. The authors speculated that “freshwater may be lost via simplified flux boundary conditions which neglect river volume inflow to the oceans”. The role of surface freshwater flux boundary conditions in global OGCMs was studied by Roulet and Madec (2000) and Tartinville et al. (2001). These studies, however, were not designed to specifically address issues relating to the Arctic Ocean, and the models had a rather coarse grid resolution (Tartinville et al. (2001) used a 3° horizontal resolution) or no sea-ice component (Roulet and Madec, 2000). Here, we utilize the regional ocean/sea-ice model COSMOS (Coupled Ocean/Sea-ice Model with Open Surface) to focus on the Arctic Mediterranean. The ‘open surface’ formulation of COSMOS accounts for dynamic surface elevation and volume fluxes due to precipitation, evaporation and river runoff. Therefore, surface freshwater forcing of the ocean is naturally implemented without the necessity of applying virtual salinity fluxes. The goal of the present work is to understand the role of surface freshwater flux boundary conditions in Arctic Ocean/sea-ice modelling. To this end, we compare a COSMOS control run (which serves as a benchmark) with the results from two modified model versions, in which a simplified surface kinematic boundary condition is used in combination with the salinity flux boundary conditions (1) and (2).

2. Model description and experimental design

The ocean/sea-ice model COSMOS has been used in previous sensitivity studies (Prange and Lohmann, 2003, 2004). For a detailed documentation of the setup and all parameters, the reader is referred to Prange (2003). Here, only a brief outline is given.

2.1. Ocean component

The oceanic component of COSMOS is based on the hydrostatic Geophysical Fluid Dynamics Laboratory (GFDL) primitive equation, z -coordinate model MOM-2 (Pacanowski, 1995). The model domain includes the Arctic Mediterranean and the Atlantic Ocean north of approximately 20° S. The model is formulated on a rotated grid to avoid the singularity of geographical coordinates at the pole (Fig. 2). It has a horizontal resolution of about 110 km (i.e., 1° on the rotated grid) and 19 non-equidistant levels in the vertical. Tracer advection employs a flux-corrected transport (FCT) algorithm (Zalesak, 1979), which eliminates undesirable computational noise (‘ripples’) within the tracer fields while reducing numerical diffusion as far as possible (Gerdes et al., 1991). Explicit tracer diffusivities are set to zero except for the convective mixing scheme (Rahmstorf, 1993) that homogenizes statically unstable sections of the water column. Summer mixed layers are thus effectively set equal to the thickness of the uppermost grid box.

For the barotropic mode of the ocean, we employ the implicit free-surface method of Dukowicz and Smith (1994), making sea-surface height η a prognostic variable. This implicit free-surface approach neglects horizontal advection of η and assumes that $|\eta| \ll \Delta z_1$, where Δz_1 denotes the thickness of the surface boxes. From this, it follows that the vertical velocity at the surface $w(z = \eta)$ can be approximated by $w_0 = w(z = 0)$. While such a linear free-surface formulation with fixed ocean thickness is not strictly tracer-conserving (cf. Griffies

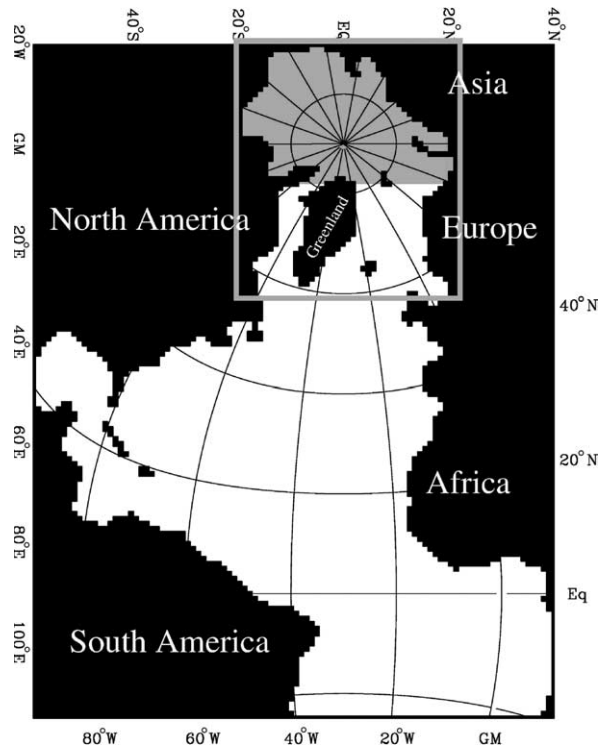


Fig. 2. Domain of the model. The model equations are defined on a rotated grid. Both the geographical and the model grid coordinates are displayed. The frame marks the region that is shown in Figs. 4, 6–10. The area of the Arctic Ocean, which is considered in the calculations of the Arctic Ocean freshwater balance, is shaded.

et al., 2001; Campin et al., 2004), the errors are small and acceptable for large-scale applications (Roulet and Madec, 2000).

In the original formulation of the linear free surface by Dukowicz and Smith (1994), vertical surface velocities can only result from the divergence of the barotropic flow field U ; that is,

$$w_0 = \frac{\partial \eta}{\partial t} = -\nabla \cdot U \quad (3)$$

(material surface). The vertical velocity w_0 must be taken into account in the baroclinic and tracer equations. Changes in surface elevation are associated with vertical advective fluxes L_0 at $z = 0$:

$$L_0(\alpha) = w_0 \alpha_1 = \frac{\partial \eta}{\partial t} \alpha_1. \quad (4)$$

Here, α_1 represents the surface value (i.e., the value in the topmost grid box) of a quantity α .

Within the framework of COSMOS, we ‘upgrade’ condition (3) to allow for the volume input and output associated with surface freshwater fluxes:

$$w_0 = \frac{\partial \eta}{\partial t} + (-P + E - R) \quad (5)$$

(non-material or ‘open’ surface). According to (4) and (5), the vertical advective salinity flux at the surface would read

$$L_0(S) = w_0 S_1 = \left(\frac{\partial \eta}{\partial t} - P + E - R \right) S_1. \quad (6)$$

Therefore, the ‘anti-advective flux’ $(-P + E - R)S_1$ must be subtracted to ensure that no salt is exchanged across the air–sea interface (Huang, 1993).

The open surface can be formulated in a more general way: Let $F_{0,n}$ be the vertical velocities across the air–sea interface (P, E, R, \dots) and let $\tilde{L}_0(\alpha)$ be the *total* flux of a quantity α (salinity, temperature, horizontal velocity, etc.) through $z = 0$, then

$$w_0 = \frac{\partial \eta}{\partial t} + \sum_n F_{0,n}, \quad (7)$$

$$\tilde{L}_0(\alpha) = \mathbf{W}_0 \cdot \mathbf{A}_1$$

with

$$\mathbf{W}_0 = \left(\frac{\partial \eta}{\partial t}, F_{0,1}, F_{0,2}, F_{0,3}, \dots \right), \quad (8)$$

$$\mathbf{A}_1 = (\alpha_1, \alpha_{1,1}, \alpha_{1,2}, \alpha_{1,3}, \dots),$$

where $\alpha_{1,n}$ denote the transported property associated with $F_{0,n}$. Considering precipitation, evaporation and river runoff with respect to salinity ($\alpha = S$), \mathbf{W}_0 and \mathbf{A}_1 are

$$\mathbf{W}_0 = \left(\frac{\partial \eta}{\partial t}, -P, E, -R \right), \quad (9)$$

$$\mathbf{A}_1 = (S_1, 0, 0, 0).$$

A passive tracer ($\alpha = C$), introduced to mark and track Arctic river runoff, is defined by

$$\mathbf{A}_1 = (C_1, 0, C_1, C_{\text{arctic}}), \quad (10)$$

where $C_{\text{arctic}} = 1$ (or 100%) for all Arctic rivers (gauged and ungauged runoff) and $C_{\text{arctic}} = 0$ for non-Arctic rivers. Note that C represents the fraction of Arctic river water in sea water; that is, Arctic river water concentration.

In order to avoid severe checkerboarding on MOM's 'B' grid, the inflow of each river is distributed equally on both sub-grids; that is, at least two adjacent coastal grid cells receive the water (cf. Mesinger, 1973). The open surface does not only allow the implementation of pure freshwater fluxes, but also the input of water with other properties. In COSMOS, the inflow of Pacific water through the Bering Strait is completely prescribed and implemented by the open surface (see Section 2.4). This relatively simple approach is justified by the strait's shallow depth (~ 50 m) relative to the thickness of the topmost model grid boxes (20 m).

The current version of the model features neither open nor sponge boundary conditions along the southern boundary of the model domain. Therefore, the model does a poor job of simulating ocean circulation and hydrography in the tropical South Atlantic. Due to the huge area of the model domain (Fig. 2), it is reasonable to assume that the effect of the southern boundary is negligible for short-term (i.e. multi-decadal) simulations of the Arctic Ocean.

2.2. Sea-ice component

The ocean model is coupled to a dynamic-thermodynamic sea-ice model which is defined on the same horizontal grid (Harder, 1996; Harder et al., 1998). The ice model employs a viscous-plastic rheology (Hibler, 1979) and includes a prognostic snow layer. The thermodynamic component of the ice model is based on the works of Semtner (1976) and Parkinson and Washington (1979), where the heat capacities of ice and snow are neglected. A compilation of all rheologic and thermodynamic parameters can be found in Prange (2003).

Outflow points are applied to the Bering Strait; that is, ice and snow which leave the model domain through this strait vanish immediately, with no freshwater being transferred to the ocean. No ice can enter the Arctic Ocean through the Bering Strait.

In order to avoid explicit diffusion in the ice model equations, advection is discretized by the positive-definite transport algorithm of Smolarkiewicz (1983). A time step of 45 min is used for all prognostic quantities of the coupled ocean/sea-ice model.

2.3. Coupling

Ocean and sea-ice are coupled through fluxes of freshwater/salt, heat and momentum. Heat and momentum fluxes are treated as in [Hibler and Bryan \(1987\)](#). Surface freshwater fluxes ($-P + E - R$) enter the ocean as volume fluxes with zero salinity according to (9). Affecting the barotropic pressure field of the ocean, these surface volume fluxes may generate oceanic currents even in the absence of density gradients. This portion of the oceanic circulation is known as the Goldsbrough circulation ([Goldsbrough, 1933](#); [Huang, 1993](#)). By way of contrast, freezing/melting phase transitions can be considered as mass exchanges between the two components of the coupled ocean/sea-ice system ([Tartinville et al., 2001](#))—no mass is added to or extracted from the ocean/sea-ice column. Therefore, freezing/melting of sea-ice does not contribute to variations of the barotropic pressure in the ocean and, hence, cannot induce a Goldsbrough circulation. We note, however, that the *movement* of sea-ice may change the barotropic pressure in the real ocean. Sea-ice drift as a source for Goldsbrough circulation is not included in the present model version. Implementation and evaluation of this effect is beyond the scope of the present study. Here, we focus on boundary conditions for ($-P + E - R$), isolating the influence of different surface freshwater flux formulations from any other factors. To account for the effect of brine rejection on sea surface salinity, we employ the salinity flux formulation

$$F_S = (S_1 - S_i)\rho' \frac{\partial h_i}{\partial t}. \quad (11)$$

S_i , ρ' , and h_i denote sea-ice salinity, ice/water density ratio, and sea-ice thickness, respectively. Sea-ice salinity is set to 3 psu. Alternative ice/ocean-coupling strategies are presented by, e.g., [Jenkins et al. \(2001\)](#) and [Schmidt et al. \(2004\)](#).

2.4. Forcing

The coupled ocean/sea-ice system is forced by fluxes of freshwater, momentum, and heat using a complete surface heat budget. Fluxes of latent and sensible heat are computed from standard bulk formulae. The prescription of shortwave insolation follows that of [Zillman \(1972\)](#); the effect of clouds is parameterized according to [Laevastu \(1960\)](#). Surface albedo distinguishes between open water (0.10), melting sea-ice (0.68), frozen sea-ice (0.70), melting snow (0.77), and frozen snow (0.81). Longwave radiation is calculated applying the Stefan–Boltzmann law, where the emissivity of the atmosphere depends on the cloud cover according to [Maykut and Church \(1973\)](#).

In order to calculate all necessary surface fluxes, atmospheric fields of 2 m-temperature, 2 m-dewpoint temperature, cloud cover, precipitation, wind speed, and wind stress are prescribed. Except for daily wind stress, all forcing fields are monthly varying. The atmospheric fields are derived from a validated 15 year (1979–1993) set of assimilated data provided by the reanalysis project of the European Center for Medium-Range Weather Forecasts (ECMWF). The data has been processed to construct a ‘typical year’; that is, a mean annual cycle with daily wind stress fluctuations superimposed ([Roeske, 2001](#)). Evaporation is diagnosed from the flux of latent heat. Precipitation falls as snow when local air temperatures drop below 0 °C.

The Bering Strait inflow is implemented by means of the open surface. For this purpose, (7) and (8) are extended, introducing a velocity, $F_{0,4}$, that corresponds to the flow through the strait. The prescribed properties of Pacific water, $\alpha_{1,4}$, are based on direct measurements by [Roach et al. \(1995\)](#). Salinity of the inflow varies between 31.5 psu in September/October and 33.5 psu in March/April. The mean volume flux is 0.8 Sv ($0.8 \times 10^6 \text{ m}^3 \text{ s}^{-1}$), but seasonal variability is considerable. Minimum fluxes in December and March are 0.3 Sv, while the maximum flux in September amounts to 1.3 Sv. The Bering Strait inflow is associated with a heat supply during the summer months. The temperature rises up to 4 °C in September, while winter temperatures (December–May) are at freezing point for the salinity.

In addition to atmospheric forcing and Bering Strait inflow, the ocean/sea-ice system is forced by river runoff. For the Atlantic portion of the model domain, the eight largest rivers are included as well as the freshwater supply from Hudson Bay and the Baltic Sea ([Prange, 2003](#)). The total freshwater supply by these sources amounts to $\sim 11 \times 10^3 \text{ km}^3 \text{ yr}^{-1}$, representing about 90% of the total runoff into the Atlantic Ocean (cf. [Grabs et al., 1996](#)). In addition, a freshwater flux of $380 \text{ km}^3 \text{ yr}^{-1}$ enters the Nordic Seas from the Norwegian coast.

Special attention is paid to the implementation of Arctic rivers. The model is forced by a monthly climatology of Arctic river runoff which has been constructed by Prange (2003). This climatology includes a total of 14 Arctic rivers, each with an annual discharge of more than 30 km^3 (Fig. 3). Based on various estimates (Plitkin, 1978; AANII/AARI, 1990; Vuglinsky, 1997), some ungauged runoff is added during summer (June–September). Along the coastlines of the Barents, Kara, and Laptev Seas, an additional freshwater inflow of $520 \text{ km}^3 \text{ yr}^{-1}$ is equally distributed. Ungauged runoff from the eastern Siberian, North American and northern Greenland coasts is smaller: a total of $180 \text{ km}^3 \text{ yr}^{-1}$ is added in these regions. Gauged and ungauged Arctic runoff therefore yields a total freshwater supply of $3159 \text{ km}^3 \text{ yr}^{-1}$.

2.5. Spin-up

The results of a 15-years spin-up run serve as initial conditions for the following sensitivity experiments. The purpose of this spin-up integration is to obtain a quasi-equilibrium field of sea-ice thickness that is consistent with the atmospheric forcing (Prange, 2003). The spin-up run is initialized with climatological data for ocean temperature and salinity (EWG (1997) for the Arctic Ocean, Levitus et al. (1994) and Levitus and Boyer (1994) outside the Arctic). Initial sea-ice concentrations are based on passive microwave observations (Gloersen et al., 1992). Initial ice thickness is set to 4 m times ice concentration, and the initial snow thickness on sea-ice is zero. During the spin-up integration, sea surface salinities are strongly restored to climatological values. This restoring is applied to the topmost grid box of the ocean model (20 m) with a time constant of 30 days. The restoring is switched off in the sensitivity experiments.

2.6. Sensitivity experiments

We perform three experiments which differ only in the boundary conditions for surface freshwater fluxes ($-P + E - R$). Experiment CTRL describes a COSMOS control run, where volume fluxes due to ($-P + E - R$) are taken into account utilizing the complete open surface formulation (7)–(10). These volume fluxes are neglected in experiments S_1 and SREF. Haline forcing is described by the virtual salinity flux (1) in experiment S_1 . In experiment SREF, the haline surface flux (2) is employed along with the commonly used reference salinity $S_{\text{ref}} = 35 \text{ psu}$.

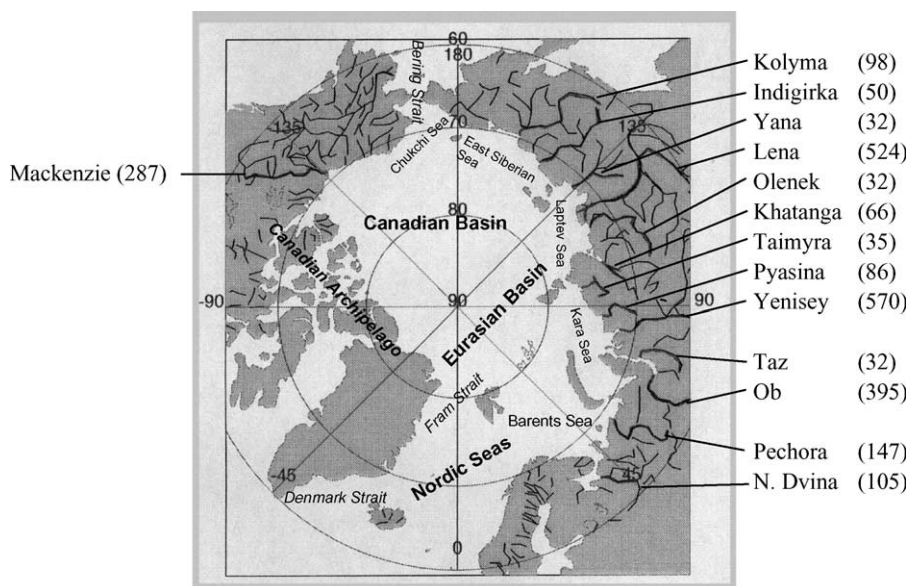


Fig. 3. Arctic rivers implemented in the model and their mean discharge in units of $\text{km}^3 \text{ yr}^{-1}$ (Prange, 2003).

Neglecting the volume input by freshwater fluxes, a passive tracer for Arctic river water concentration is introduced by the virtual surface flux

$$F_C = R(C_{\text{arctic}} - C_1) - PC_1 \quad (12)$$

into the ocean in both experiment S_1 and experiment SREF. Within the framework of the approximation, this approach is consistent with definition (10) used in experiment CTRL.

For a direct comparison of the results, all experiments are started from the same spin-up (cf. Section 2.5). Initial Arctic river water concentrations are set to zero everywhere in the ocean. For each sensitivity experiment the model is integrated for another 30 years. It is important to note that the three sensitivity experiments are performed in a prognostic mode; that is, no restoring fluxes are applied to force the model.

3. Results

The total model domain represents a net evaporative basin. Integrating $(-P + E - R)$ over the entire area yields a net evaporative flux of about 0.79 Sv. Since the model does not include a compensating oceanic freshwater transport across the southern boundary of the domain, the mean salinity slowly increases during the experiments. In experiments CTRL and SREF, the mean salinity increases by 0.1 psu during the 30 years of integration. In experiment S_1 , the salinity build-up is somewhat larger (0.12 psu in 30 years) as a result of the non-conservative nature of boundary condition (1). The positive salinity trend produced by the missing freshwater inflow along the southern model boundary slowly propagates northward but hardly reaches the Arctic realm within the integration period.

In the following, annual-mean fields from the last year of the integration period are presented. We focus on the upper Arctic Ocean, where the differences between the experiments are largest. For a more detailed presentation of the control simulation, the reader is referred to Prange (2003).

3.1. Control run

The oceanic circulation of experiment CTRL, averaged over the topmost 80 m, is shown in Fig. 4a for the polar and subpolar seas. The upper 80 m are represented by the three topmost levels of the model grid and comprise the surface mixed layer with the upper part of the cold halocline in the Arctic Ocean. The model captures important features of the observed flow pattern. A strong cyclonic gyre dominates the Nordic Seas, consisting of the EGC (East Greenland Current) in the west, and the NAC (Norwegian Atlantic Current) in the east. The latter carries warm water from the Atlantic to the north, while the EGC brings cold and fresh polar water to the south, where it leaves the Nordic Seas through Denmark Strait. Atlantic water enters the

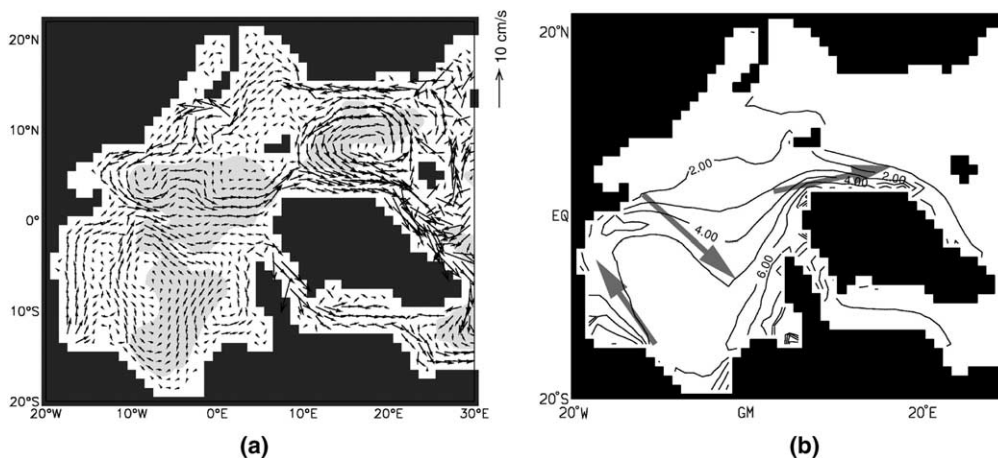


Fig. 4. (a) Mean upper ocean velocity (averaged over the topmost 80 m) and (b) mean sea-ice thickness (m) in the last year of experiment CTRL. The arrows in (b) indicate directions of the 'typical year' mean wind stress. Labels refer to the rotated model grid.

Barents Sea, transporting heat into the Arctic Ocean proper. This current constitutes the southern branch of an overall cyclonic flow pattern in the eastern Arctic Ocean. The Canadian Basin in the western Arctic is dominated by the anticyclonic Beaufort Gyre. The western anticyclonic gyre meets the eastern cyclonic circulation in the central Arctic, thereby forming the current system of the Transpolar Drift (TPD). The TPD carries polar waters towards the outlets of the Arctic Ocean, namely Fram Strait and Nares Strait (Canadian Arctic Archipelago). The West Spitsbergen Current (WSC) is absent in the upper ocean layers of the model. The model version of the WSC enters the Arctic Ocean between 250 and 700 m depth. Similarly deep inflows have been found in other prognostic ocean/sea-ice models (Häkkinen and Mellor, 1992; Zhang et al., 1998).

The annual-mean net Atlantic inflow to the Barents Sea through the Svalbard-Norway passage amounts to 1.4 Sv in the model, which is in accordance with recent estimates based on multi-year current meter measurements (Ingvaldsen et al., 2004). The modelled flow through the Canadian Arctic Archipelago is 0.8 Sv. Unfortunately, there are not enough observational data from this region to specify a typical volume transport through the archipelago. Published values lie between 0.5 and 2.7 Sv (Melling, 2000) and, hence, the volume flux in our simulation does not seem unrealistic. However, it is important to realize that, in reality, the outflow of polar water masses is distributed over a multitude of narrow channels with a total width of ~ 120 km (Melling, 2000). In the model, the entire flow through the archipelago takes place through the Nares Strait which is unrealistically wide (~ 200 km instead of ~ 30 km). Volume fluxes into and out of the Arctic Ocean through the Barents Sea, the Canadian Arctic Archipelago, the Bering Strait, and rivers are balanced by a mean net outflow of 1.5 Sv through Fram Strait.

The modelled mean ice drift resembles the upper ocean circulation, comprising an anticyclonic gyre over the Canadian Basin, a TPD, outflow through Fram Strait and an EGC (not shown). Fig. 4b displays the field of sea-ice thickness. In accordance with upward looking sonar observations (e.g., Bourke and Garrett, 1987) and satellite altimeter measurements (Laxon et al., 2003), maximum ice thicknesses are found north of Canada; ice thicknesses decrease towards Siberia. The largest discrepancy between model and data is found over the Canadian Basin where the model predicts an annual-mean sea-ice thickness of about 5 m, while measurements suggest a thickness of only 2–4 m. The tongue of thick sea-ice, extending from Canada to the East Siberian Sea (Fig. 4b) can mainly be attributed to the wind stress forcing of the ‘typical year’. The annual-mean wind pattern is characterized by an anticyclonic circulation, the center of which is located far in the west (see Figure V.2 in Prange, 2003). Consequently, mean wind stress vectors over the central Arctic are directed from the Laptev Sea towards the western islands of the Canadian Arctic Archipelago (see arrows in Fig. 4b). This wind stress pattern forces considerable portions of sea-ice in the central Arctic to drift towards the Canadian Basin (rather than towards Fram Strait) thereby maintaining an unusually thick ice-cover in that region. An equilibrium ice thickness is achieved through the action of internal sea-ice forces. Fig. 5 shows the temporal evolution of total Arctic sea-ice volume. The quasi-equilibrium state after 30 years of integration has an annual-mean total ice volume of about $37 \times 10^3 \text{ km}^3$.

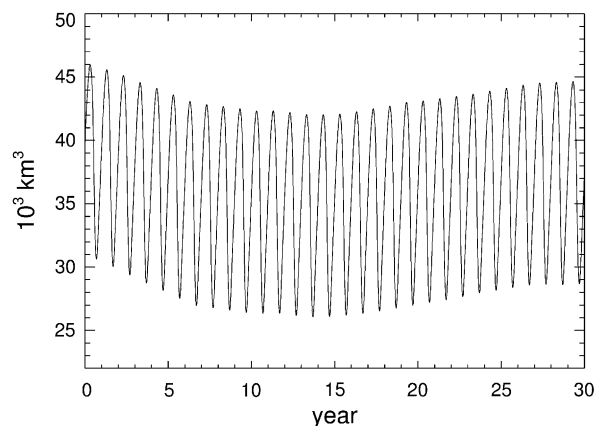


Fig. 5. Time evolution of the total sea-ice volume in experiment CTRL.

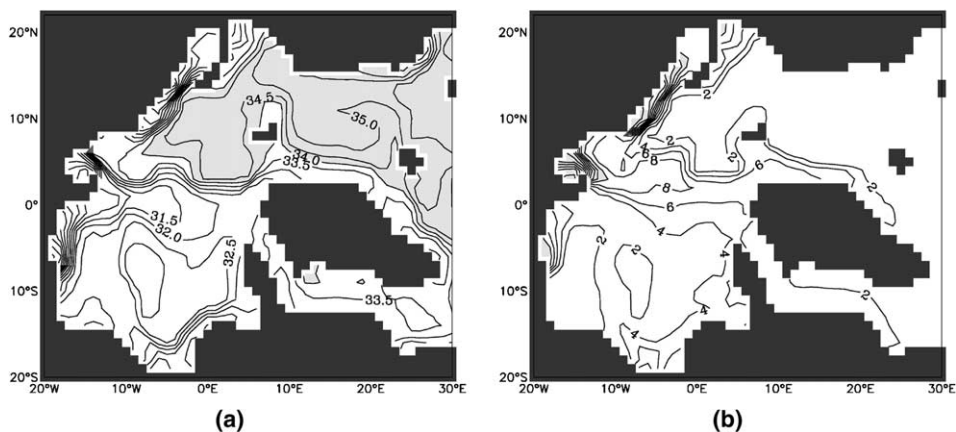


Fig. 6. Mean upper ocean fields (averaged over the topmost 80 m) from the last year of experiment CTRL: (a) salinity (psu) and (b) Arctic river water concentration (%). Regions with values larger than 34 psu and 10%, respectively, are shaded. Labels refer to the rotated model grid.

Table 1

Differences between modelled salinities and observations (PHC 2.1, updated from Steele et al. (2001b))

Region	Experiment CTRL	Experiment S_1	Experiment SREF
Canada Basin	1.18	1.73	1.21
Makarov Basin	0.04	0.86	0.12
Amundsen Basin	-0.04	0.74	0.15
Nansen Basin	-0.20	-0.18	-0.31

All values represent annual-mean salinities (psu) averaged over the top 80 m of an entire basin.

Fig. 6 shows the fields of salinity and Arctic river water concentration within the top 80 m of the high-latitude ocean. High salinities in the Norwegian and Barents Seas indicate the inflow of Atlantic water from the south (Fig. 6a). In the Arctic Ocean proper, salinities are much lower with minima in the Siberian shelf seas due to inflowing river water (Fig. 6b). Low-saline shelf waters are advected into the central Arctic Ocean, eventually leaving the Arctic Ocean through Fram Strait and the Canadian Archipelago. Melting sea-ice and the southward flow of polar water in the EGC cause low salinities in the western Nordic Seas. In the central Canadian Basin, we find modelled surface salinities to be significantly higher than observed values, resulting in a local salinity maximum which has no counterpart in observational data (cf. Steele et al., 2001b). This is a common and still unsolved problem in prognostic Arctic Ocean modelling (Steele et al., 2001a). Part of this model-data discrepancy might be explained by unresolved eddies (10–20 km diameter) which transport fresh shelf-sea waters towards the deep basins of the Arctic Ocean (cf. Hunkins, 1974). Differences between simulated salinities and observations for the deep basins of the Arctic Ocean are summarized in Table 1.

In the western Fram Strait the mean upper-ocean concentration of Arctic river water is 6–7%. Arctic river water is absent in the Norwegian and Chukchi Seas, which are dominated by inflowing waters from the Atlantic and Pacific, respectively. In the Eurasian Basin, the model results are in reasonable agreement with meteoric water distributions inferred from measurements of stable oxygen isotopes in Arctic sea water (e.g., Bauch et al., 1995). In the Canadian Basin, modelled river runoff fractions are smaller than ‘observational’ data (Ekwurzel et al., 2001), consistent with relatively high salinities.

3.2. Using virtual salinity fluxes

The use of virtual salinity flux boundary condition (1) in experiment S_1 results in an overall saltier Arctic Ocean compared to the control simulation (Fig. 7a). Neglecting the volume input of surface freshwater fluxes leads to salinity increases of more than 0.5 psu in the topmost layers of the Canadian Basin, 0.5–1 psu in the

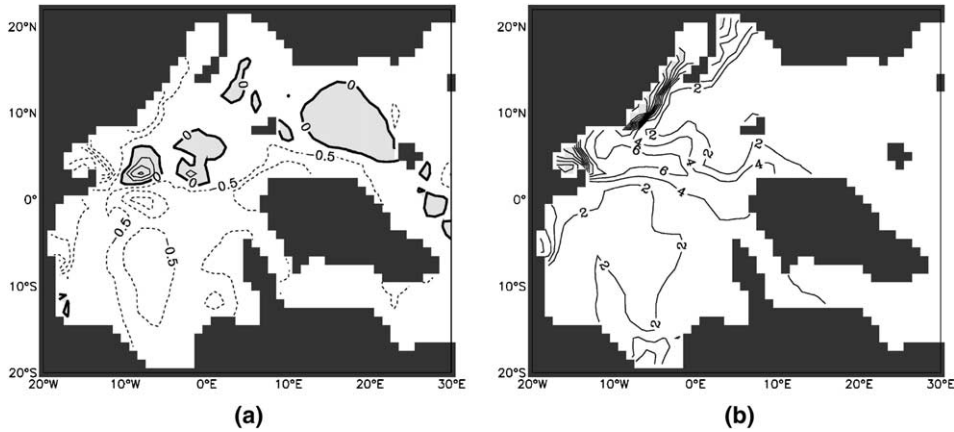


Fig. 7. Mean upper ocean fields (averaged over the topmost 80 m) from the last year of experiment S_1 : (a) salinity deficit compared to experiment CTRL (contour interval is 0.5 psu) and (b) Arctic river water concentration (%). Regions with values larger than 0 psu and 10%, respectively, are shaded. Labels refer to the rotated model grid.

EGC, 1 psu in the Kara and East Siberian Seas, and up to 3 psu in the Laptev Sea. The overall agreement with observed salinities is poor (Table 1). Fig. 7b reveals that the input of river water is strongly reduced in experiment S_1 . Compared to CTRL (Fig. 6b), river water concentrations in the upper 80 m of the Arctic Ocean are significantly smaller.

Differences in sea-water density are associated with changes in the upper ocean circulation (Fig. 8a). A slackening of the anticyclonic Beaufort Gyre in experiment S_1 is consistent with saltier conditions in the Canadian Basin (cf. Zhang et al., 1998). Moreover, the path of the TPD is affected by the freshwater boundary conditions, as the current is shifted to the west in experiment S_1 , while the outflow of polar water through Fram Strait is weakened. A saltier EGC in experiment S_1 (Fig. 7a) is associated with a slower surface current. Therefore it appears that the EGC is, at least partially, driven by freshwater-induced density gradients. Note also the changes in the cyclonic flow pattern of the Nordic Seas, prominent in Fig. 8a.

Changes in oceanic circulation and hydrography influence polar sea-ice by dynamic and thermodynamic processes. The drift of sea-ice is coupled to ocean currents through ocean/sea-ice stresses. Therefore, differences in sea-ice motion between the experiments resemble differences in the upper ocean circulation displayed in Fig. 8a. An overall larger ice thickness in the control run (Fig. 8b) can be attributed to reduced upward

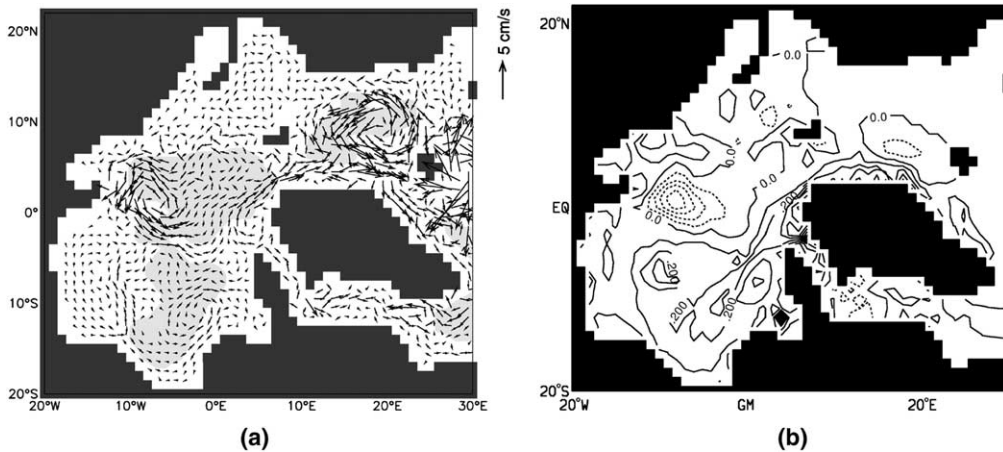


Fig. 8. Experiment CTRL minus experiment S_1 : (a) mean velocity difference (averaged over the topmost 80 m) and (b) mean ice thickness difference (contour interval is 0.1 m) in the last year of the integration period. Labels refer to the rotated model grid.

ocean-ice heat fluxes which are controlled by the oceanic density stratification. Fresher surface conditions in experiment CTRL tend to stabilize the cold halocline that shields the surface from the warm Atlantic layer below (cf. Steele and Boyd, 1998). However, since both simulations feature a distinct cold halocline layer, differences in ocean-ice heat fluxes and hence sea-ice thickness are small between experiment S_1 and CTRL. The annual-mean upward ocean-ice heat flux averaged over the Arctic Ocean (as defined by the shaded area in Fig. 2) in experiment S_1 is only 0.12 W m^{-2} greater than in the control run.

Introducing a reference salinity $S_{\text{ref}} = 35$ psu in the definition of the salinity flux boundary condition results in hydrographic fields which are much more similar to those of the control run (cf. Table 1). Comparing experiment SREF with CTRL, we find significant differences in upper-ocean salinity only at few locations (Fig. 9a). Accordingly, differences in the fields of velocity and sea-ice thickness are small (Fig. 10). The most striking shortcoming in experiment SREF is revealed by looking at the concentration of Arctic river water (Fig. 9b). The simulation of river water distribution in the Arctic Ocean is as poor as in experiment S_1 .

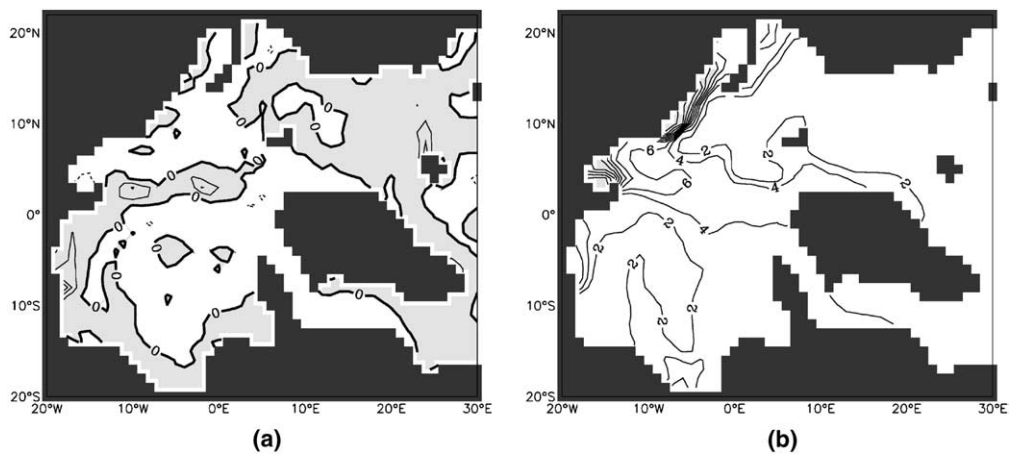


Fig. 9. Mean upper ocean fields (averaged over the topmost 80 m) from the last year of experiment SREF: (a) salinity deficit compared to experiment CTRL (contour interval is 0.5 psu) and (b) Arctic river water concentration (%). Regions with values larger than 0 psu and 10%, respectively, are shaded. Labels refer to the rotated model grid.

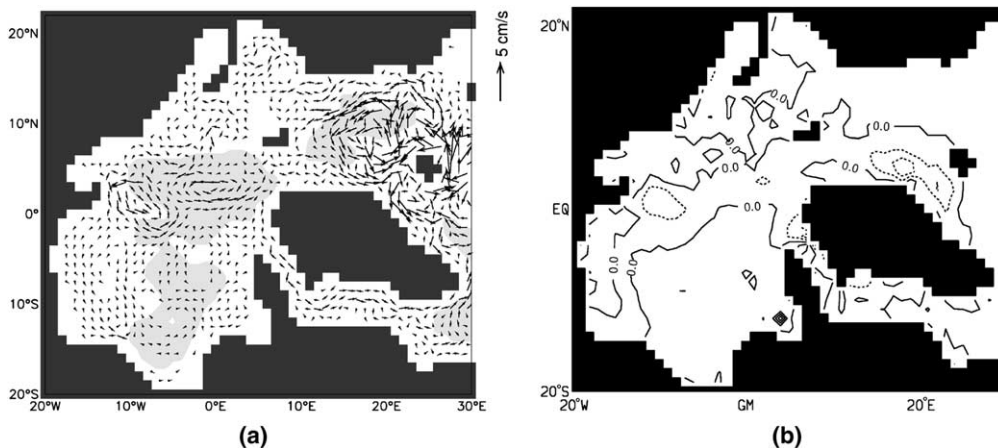


Fig. 10. Experiment CTRL minus experiment SREF: (a) mean velocity difference (averaged over the topmost 80 m) and (b) mean ice thickness difference (contour interval is 0.1 m) in the last year of the integration period. Labels refer to the rotated model grid.

4. Discussion

4.1. Salinity flux boundary conditions: What is missing?

The high surface salinities in experiment S_1 (Fig. 7a) suggest that the freshwater forcing is too weak when the salinity flux condition (1) is used. Fig. 11 shows the time evolution of mean salinity in the Arctic Ocean during the 30 years of model integration. While in experiments CTRL and SREF Arctic mean salinity reaches a quasi-equilibrium at the end of the integration period, a strong salinity drift in experiment S_1 indicates that the Arctic Ocean gains salt, such that the hydrography gets more and more unrealistic with increasing integration time. What is missing?

In order to understand how freshwater enters the model ocean in the different experiments, we consider the time evolution of a quantity α (e.g., salinity, river water concentration) in an infinite line of ocean grid boxes (Fig. 12). The grid boxes have constant volumes (all dimensions are set to 1) and are connected with each other by advective fluxes. The ‘channel’ is isolated and surrounded by rigid walls, except for an input of river water into the first box ($i = 1$) with a constant rate Q . This input induces a steady, divergence-free flow of the incompressible fluid, the volume flux of which is Q . Applying a simple upstream scheme for advection, the evolution of α in box i can be described by

$$\frac{d\alpha_i}{dt} = Q(\alpha_{i-1} - \alpha_i) = Q(\alpha_0 - \alpha_i) - \sum_{n=1}^{i-1} \frac{d\alpha_n}{dt}. \tag{13}$$

Here, α_0 is the constant value of α for the inflowing river water. (13) can be solved for the initial condition $\alpha_i(t = 0) = 0$ for all i :

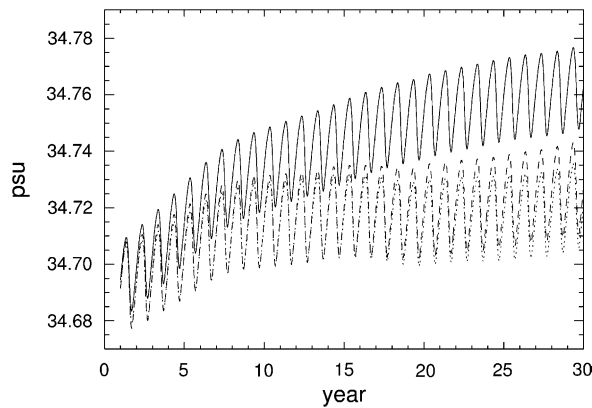


Fig. 11. Time evolution of mean salinity in the Arctic Ocean (shaded area in Fig. 2) in experiment CTRL (dotted), experiment S_1 (solid), and experiment SREF (dashed).

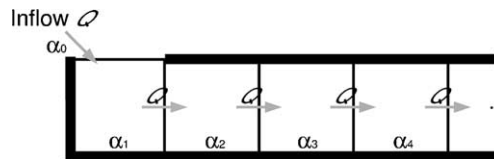


Fig. 12. Upstream ‘box model’: The grid boxes are connected with each other by advective fluxes. The ‘channel’ is isolated and surrounded by rigid walls, except for an input of river water into the first box with a constant rate Q . This input induces a steady, divergence-free flow of the incompressible fluid.

$$\alpha_i(t) = \alpha_0 - \alpha_0 e^{-Qt} \sum_{n=1}^i \frac{1}{(n-1)!} (Qt)^{(n-1)}. \quad (14)$$

For $i = 1, 2, 3$ and $\alpha_0 = Q = 1$ the solution is plotted in Fig. 13. The inflowing volume flux Q has an effect on *all* ocean boxes, since α_0 is transferred by advection.

Implementing the river inflow by a salinity flux condition, analogous to Eqs. (1) and (12), the temporal evolution of our conceptual model reads

$$\begin{aligned} \frac{d\alpha_1}{dt} &= Q(\alpha_0 - \alpha_1), \\ \frac{d\alpha_i}{dt} &= 0 \quad \text{for } i > 1. \end{aligned} \quad (15)$$

Here, the effect of Q is limited to the first box; that is, the river water input Q is not felt by the other boxes ($i > 1$). In other words, the lack of advective terms in the system of Eq. (15) results in a loss of river water when a salinity flux boundary condition is used. Concerning the freshwater budget of the ‘box model’, the poor implementation of river water leads to excessive salinities. The same applies to the OGCM in experiment S_1 , provided that box $i = 1$ represents coastal grid cells located at river mouths, and the flow Q through the ‘channel’ stands for the barotropic circulation in the OGCM that is induced by surface volume fluxes; that is, the Goldsbrough flow (Goldsbrough, 1933). Even though the volume input of rivers is small compared to typical volume transports inside the ocean, it must be taken into account in order to deliver sufficient amounts of freshwater to the grid boxes of the OGCM. The same holds for precipitation, however, river runoff is much more important for the Arctic Ocean freshwater budget (see below).

The advent of a constant reference salinity for surface salinity fluxes in experiment SREF leads to an improvement of the simulation, with Arctic surface salinities being significantly lower than in experiment S_1 . Since $S_{\text{ref}} = 35$ psu is considerably larger than typical surface salinities close to Arctic river mouths, surface salinity fluxes are effectively overestimated in experiment SREF. However, it is important to realise that the choice of the reference salinity is arbitrary. If S_{ref} is set too small, the Arctic Ocean will become too salty; if S_{ref} is too large, the ocean will be too fresh. By chance, a value of $S_{\text{ref}} = 35$ psu works well in our model setup. In other words, experiment SREF yields the ‘right result’ for the wrong reason.

Our simple analytical model considers the specific situation of the Arctic Ocean basin, where the freshwater forcing is mostly composed of river discharge along the lateral margins, and where—except for a small area in the western Barents Sea—there are no regions of net evaporation (hence, only freshwater *input* is included). The analytical model can easily be extended by adding evaporative boxes (i.e. freshwater *output*) in order to show that, in a more general framework, the absence of the Goldsbrough circulation causes non-conservation of salinity when boundary condition (1) is employed.

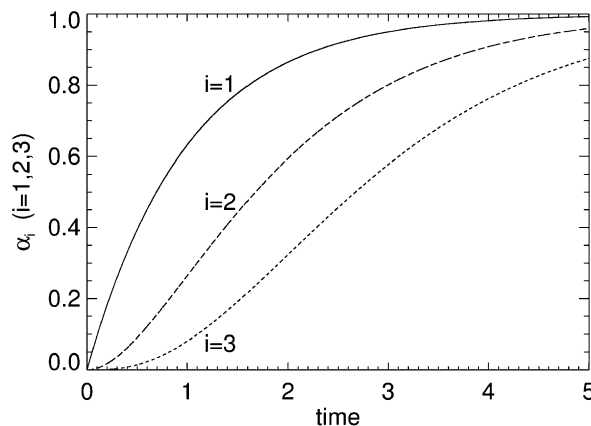


Fig. 13. Solution of the upstream ‘box model’ for $i = 1, 2, 3$ ($\alpha_0 = 1$, $Q = 1$; $\alpha_i(t = 0) = 0$).

4.2. Freshwater balance of the Arctic Ocean

Evaluation of freshwater transports and the Arctic Ocean freshwater balance provides further insight into the role of surface freshwater flux boundary conditions. For a quantitative evaluation of the Arctic Ocean freshwater balance, a reference salinity has to be defined. For this purpose, it is reasonable to regard Atlantic water as an ‘original water mass’, filling the Arctic Ocean from the south and then being diluted by inflowing freshwater. Water masses, leaving the Arctic Ocean, can then be considered as a mixture of Atlantic water with freshwater. Therefore, the most reasonable choice for a reference salinity is the salinity of the Atlantic inflow, $S_{\text{atl}} \approx 35$ psu. The fraction of pure freshwater in Arctic sea water is then given by $(S_{\text{atl}} - S)/S_{\text{atl}}$.

Table 2 shows the freshwater balances of the Arctic Ocean based on the last year of experiments CTRL, S_1 and SREF, using the reference salinity $S_{\text{ref}} = S_{\text{atl}} = 35$ psu. The corresponding area of the Arctic Ocean and the locations of the passages are displayed in Fig. 2. Since neither the ocean model nor the sea-ice model include explicit diffusion, all transports are purely advective. For an accurate calculation, advective transports were taken directly from the advection subroutines of the model code at each time step. The export of sea-ice through the Bering Strait (where the ice model possesses outflow points) and transports of snow drifting on the ice are neglected in Table 2 (values are lower than $50 \text{ km}^3 \text{ yr}^{-1}$). Even when including these numbers, none of the experiments yields a vanishing remaining sum in the freshwater balance. In fact, one cannot expect a completely balanced freshwater budget of the Arctic Ocean after 30 years of integration, mainly due to a slow salinity drift within the Arctic intermediate and deep layers where the mean residence time of water masses is much larger than the $O(10)$ years typical for the Arctic halocline (cf. Schlosser et al., 1999).

In addition to the model results, estimates based on observations are listed in Table 2 (right column). These values are recalculated from the data given in the pioneering work of Aagaard and Carmack (1989). For this recalculation, we employ the reference salinity $S_{\text{ref}} = 35$ psu and assume the same sea-ice salinity as in the model, $S_i = 3$ psu (Aagaard and Carmack (1989) applied $S_{\text{ref}} = 34.8$ psu and $S_i = 4$ psu in their original paper). The recalculation permits a direct comparison between model and data. In experiments CTRL and SREF significant differences are only found in the Barents Sea, where the data suggest an input of freshwater to the Arctic Ocean, while a net loss of freshwater is computed by the model. We suppose that this discrepancy may partly be attributed to the low-saline Norwegian Coastal Current (NCC), which constitutes an important freshwater source for the Barents Sea in the estimates of Aagaard and Carmack (1989): On the basis of hydrographic and current measurements, Aagaard and Carmack (1989) assume a transport of 0.7 Sv into the Barents Sea within a narrow coastal wedge of low-salinity water (34.4 psu) off northern Norway. This distinct

Table 2

Freshwater balance of the Arctic Ocean based on experiments CTRL, S_1 , and SREF (averaged over the last year of each integration period) and values based on observations (Aagaard and Carmack, 1989)

Sources/sinks	Experiment CTRL	S_1	SREF	Observ.
$P - E$	$1895 - 508 = 1387$	1359	1377	900
Rivers	3159	3159	3159	3300
Bering Strait	1771	1771	1771	1800
Barents Sea				
Sea-ice	−316	−295	−296	–
Liquid water	−417	−582	−366	270
Fram Strait				
Sea-ice	−2952	−2614	−2849	−2880
Liquid water	−1572	−572	−1336	−1330
Canadian Archipelago				
Sea-ice	−180	−206	−159	−140
Liquid water	−1393	−1092	−1157	−1220
Sum	−513	928	144	700

A reference salinity of 35 psu is used along with a sea-ice salinity of 3 psu. Positive values denote net import of freshwater, negative values denote net export of freshwater with respect to the shaded area marked in Fig. 2. All transports are given in $\text{km}^3 \text{ yr}^{-1}$.

low-saline current along the coast of northern Norway is not resolved in our ocean model (cf. Fig. 6a) so that the total freshwater supply to the Barents Sea is likely to be underestimated.

The total freshwater input to the Arctic Ocean by runoff, precipitation and Bering Strait inflow is approximately $6800 \text{ km}^3 \text{ yr}^{-1}$ in our model setup. The freshwater outflows via the Barents Sea, Fram Strait, and the Canadian Archipelago are very similar between experiments CTRL and SREF. In both experiments about 20% of the total Arctic freshwater input is exported by ocean currents through Nares Strait. Since this strait is too wide in our model, we interpret this throughflow as the freshwater export through the Canadian Arctic Archipelago as a whole. The simulation of a realistic freshwater flow through the archipelago is of utmost

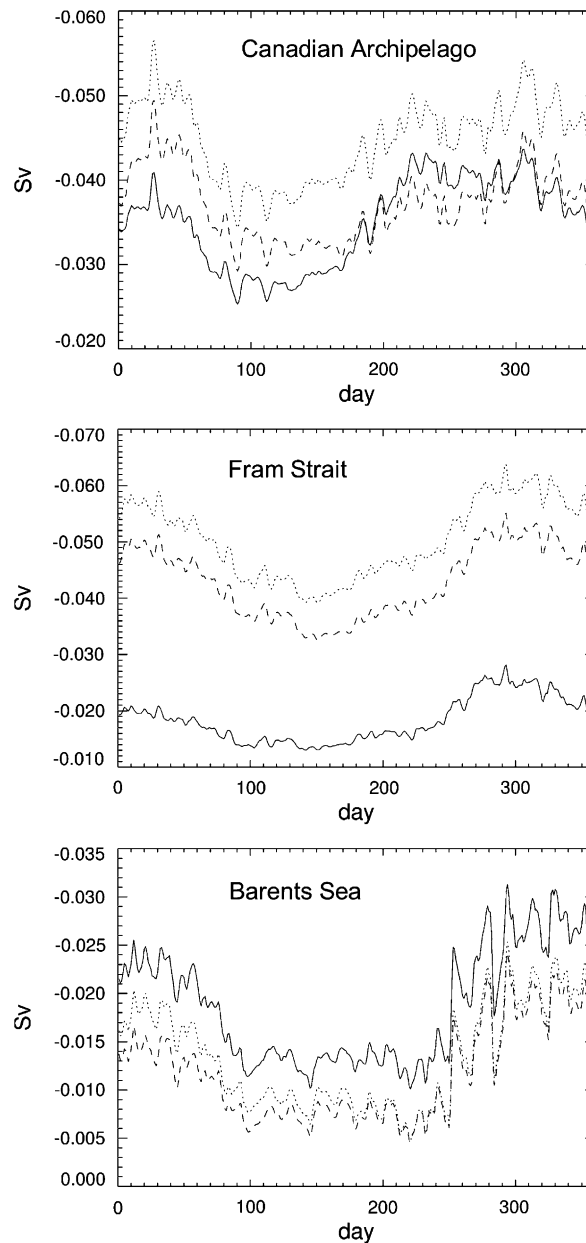


Fig. 14. Oceanic freshwater transports through the Canadian Archipelago, the Fram Strait and the Barents Sea during the last year of the integration periods (smoothed by a 30-days-boxcar-average) of experiments CTRL (dotted), S_1 (solid), and SREF (dashed). Negative values denote transports out of the Arctic Ocean.

importance in a prognostic Arctic Ocean model, since an overestimation of this flow would most likely be on the cost of Fram Strait freshwater export. In both experiment CTRL and experiment SREF, it provides confidence that the simulated freshwater export through the Canadian Archipelago is consistent not only with the data of Aagaard and Carmack (1989), but also with a simple model study by Steele et al. (1996).

The freshwater balance of experiment S_1 reveals a less successful simulation. In Fram Strait, the oceanic freshwater export in experiment S_1 is $1000 \text{ km}^3 \text{ yr}^{-1}$ smaller than in the control run owing to higher salinity and weaker flow. Along with lower sea-ice export and Canadian Archipelago freshwater throughflow this results in a large positive remaining sum of $928 \text{ km}^3 \text{ yr}^{-1}$ in the freshwater balance (Table 2). Nevertheless, Arctic Ocean mean salinity increases in experiment S_1 (Fig. 11), which again reflects the non-conservative nature of boundary condition (1). Fig. 14 shows the annual cycle of oceanic freshwater transports through the different outlets of the Arctic Ocean for all experiments.

The implementation of a river water tracer provides further insight into the pathways of freshwater transport in our model. Analysing the advection of Arctic river water from experiment CTRL, we find that one-third of this water leaves the Arctic Ocean via the Canadian Archipelago, while almost two-thirds flow out through Fram Strait. Calculating the inventory of river water in the Arctic halocline by integrating C over the upper 300 m of the Arctic Ocean, we find a total storage of $46 \times 10^3 \text{ km}^3$ in the control run. Dividing this value by the inflow of Arctic river water (i.e., $3159 \text{ km}^3 \text{ yr}^{-1}$) yields an average mean residence time of 14–15 years for river water within the Arctic halocline. This model result agrees well with previous estimates, based on observational data (e.g., Bauch et al., 1995).

It is important to note that the freshwater balance of the Arctic Ocean may be subject to considerable inter-annual and decadal variability (e.g., Steele et al., 1996; Koeberle and Gerdes, 2003). Since the forcing in our model setup is provided by a ‘typical year’, the analyses presented in this section should be understood in a climatological sense.

5. Conclusions

The present study highlights the importance of surface freshwater flux boundary conditions in Arctic Ocean/sea-ice modelling. In COSMOS, the inflows of river water and other freshwater sources are implemented by a surface boundary condition that accounts for the input of volume (‘open surface’). With respect to surface forcing, COSMOS is therefore superior to models of the Arctic Mediterranean which are driven by ‘virtual salinity fluxes’. Simply neglecting the volume input of surface freshwater fluxes, i.e. applying boundary condition (1), leads to significant salinity increases in the upper Arctic Ocean. The associated differences in sea-water density have implications for the oceanic circulation, which are particularly pronounced in the outflow of polar water via the EGC. These findings may help to interpret the results of previous model studies.

Our results further suggest that virtual salinity fluxes in combination with a fixed reference salinity are a reasonable approximation for Arctic Ocean models with horizontal resolution comparable to our model. Introducing a reference salinity of $S_{\text{ref}} = 35 \text{ psu}$ in the definition of salinity flux boundary condition (2) results in hydrographic fields and freshwater transports which are similar to those from the control run with open surface. If, for technical reasons, the use of virtual salinity flux boundary conditions cannot be avoided, we therefore recommend applying formulation (2) with $S_{\text{ref}} = 35 \text{ psu}$ rather than formulation (1). We point out, however, that physically consistent boundary conditions, which take the fluxes of volume into account, should be applied for the simulation of tracers like river water concentration or isotopic signals of meteoric water.

Acknowledgements

This manuscript was put together while RG spent a sabbatical at the Geophysical Fluid Dynamics Laboratory, Princeton. RG thanks GFDL for the hospitality and financial support. MP thanks Michael Schulz for his support. Stimulating discussions with Cornelia Koeberle, Michael Karcher and Dirk Olbers are gratefully acknowledged. The constructive comments by Peter Killworth and two anonymous reviewers are highly appreciated. Part of this work was funded by the German Bundesministerium für Bildung und Forschung

through the DEKLIM project, and by the Deutsche Forschungsgemeinschaft through the DFG Research Center ‘Ocean Margins’ at the University of Bremen (No. RCOM0327).

References

- Aagaard, K., Carmack, E.C., 1989. The role of sea ice and other fresh water in the Arctic circulation. *J. Geophys. Res.* 94, 14485–14498.
- AANII/AARI, 1990. Estimate of river inflow to the Karsk Sea and its annual and seasonal variation. AANII Report, Arctic-Antarctic Nauchno-Issled. Inst., Leningrad (St. Petersburg).
- Barnier, B., 1998. Forcing the ocean. In: Chassignet, E.P., Verron, J. (Eds.), *Ocean Modeling and Parameterization*. Kluwer Academic Publishers, Netherlands, pp. 45–80.
- Bauch, D., Schlosser, P., Fairbanks, R.G., 1995. Freshwater balance and the sources of deep and bottom waters in the Arctic Ocean inferred from the distribution of $H_2^{18}O$. *Prog. Oceanogr.* 35, 53–80.
- Bourke, R.H., Garrett, R.P., 1987. Sea ice thickness distribution in the Arctic Ocean. *Cold Reg. Sci. Technol.* 13, 259–280.
- Campin, J.-M., Adcroft, A., Hill, C., Marshall, J., 2004. Conservation of properties in a free-surface model. *Ocean Model.* 6, 221–244.
- Dukowicz, J.K., Smith, R.D., 1994. Implicit free-surface method for the Bryan–Cox–Semtner Ocean Model. *J. Geophys. Res.* 99, 7991–8014.
- Ekwurzel, B., Schlosser, P., Mortlock, R., Fairbanks, R., Swift, J.H., 2001. River runoff, sea ice meltwater, and Pacific water distribution and mean residence times in the Arctic Ocean. *J. Geophys. Res.* 106, 9075–9092.
- EWG (Environmental Working Group), 1997. Joint US–Russian Atlas of the Arctic Ocean. CD-ROM, Natl. Snow and Ice Center, Boulder.
- Gerdes, R., Koeberle, C., Willebrand, J., 1991. The influence of numerical advection schemes on the results of ocean general circulation models. *Climate Dyn.* 5, 211–226.
- Gloersen, P., Campbell, W.J., Cavalieri, D.J., Comiso, J.C., Parkinson, C.L., Zwally, H.J., 1992. Arctic and Antarctic Sea Ice, 1978–1987: Satellite Passive-Microwave Observations and Analysis. NASA SP-511, Washington, DC.
- Goldsbrough, G., 1933. Ocean currents produced by evaporation and precipitation. *Proc. Roy. Soc. Lond. A* 141, 512–517.
- Grabs, W., De Couet, T., Pauler, J., 1996. Freshwater fluxes from continents into the world oceans based on data of the Global Runoff Data Base. GRDC Report, 10, Global Runoff Data Centre, Federal Institute of Hydrology, Koblenz, Germany.
- Gregory, J.M., Huybrechts, P., Raper, S.C.B., 2004. Threatened loss of the Greenland ice-sheet. *Nature* 428, 616.
- Griffies, S.M., Pacanowski, R.C., Schmidt, M., Balaji, V., 2001. Tracer conservation with an explicit free surface method for z-coordinate ocean models. *Mon. Weather Rev.* 129, 1081–1098.
- Häkkinen, S., Mellor, G.L., 1992. Modeling the seasonal variability of a coupled Arctic ice-ocean system. *J. Geophys. Res.* 97, 20285–20304.
- Häkkinen, S., 1999. A simulation of thermohaline effects of a Great Salinity Anomaly. *J. Climate* 12, 1781–1795.
- Harder, M., 1996. Dynamik, Rauigkeit und Alter des Meereises in der Arktis—Numerische Untersuchungen mit einem großskaligen Modell. *Rep. Polar Res.*, 203, AWI, Bremerhaven, Germany.
- Harder, M., Lemke, P., Hilmer, M., 1998. Simulation of sea ice transport through Fram Strait—natural variability and sensitivity to forcing. *J. Geophys. Res.* 103, 5595–5606.
- Hibler, W.D., 1979. A dynamic thermodynamic sea ice model. *J. Phys. Oceanogr.* 9, 815–846.
- Hibler, W.D., Bryan, K., 1987. A diagnostic ice-ocean model. *J. Phys. Oceanogr.* 17, 987–1015.
- Holland, D.M., Mysak, L.A., Oberhuber, J.M., 1996. Simulation of the mixed-layer circulation in the Arctic Ocean. *J. Geophys. Res.* 101, 1111–1128.
- Holloway, G., Sou, T., 2002. Has Arctic sea ice rapidly thinned? *J. Climate* 15, 1691–1701.
- Huang, R.X., 1993. Real freshwater flux as a natural boundary condition for the salinity balance and thermohaline circulation forced by evaporation and precipitation. *J. Phys. Oceanogr.* 23, 2428–2446.
- Hunkins, K.L., 1974. Subsurface eddies in the Arctic Ocean. *Deep Sea Res.* 21, 1017–1033.
- Ingvaldsen, R.B., Asplin, L., Loeng, H., 2004. The seasonal cycle in the Atlantic transport to the Barents Sea during the years 1997–2001. *Cont. Shelf Res.* 24, 1015–1032.
- Jenkins, A., Hellmer, H.H., Holland, D.M., 2001. The role of meltwater advection in the formulation of conservative boundary conditions at an ice-ocean interface. *J. Phys. Oceanogr.* 31, 285–296.
- Koeberle, C., Gerdes, R., 2003. Mechanisms determining the variability of Arctic sea ice conditions and export. *J. Climate* 16, 2843–2858.
- Laevastu, T., 1960. Factors affecting the temperature of the surface layer of the sea. *Comment Phys. Math.* 25/1.
- Laxon, S., Peacock, N., Smith, D., 2003. High interannual variability of sea ice thickness in the Arctic region. *Nature* 425, 947–950.
- Levitus, S., Boyer, T., 1994. *World Ocean Atlas 1994, Vol. 4: Temperature*. NOAA Atlas NESDIS 4, US Gov. Printing Office.
- Levitus, S., Burgett, R., Boyer, T., 1994. *World Ocean Atlas 1994, Vol. 3: Salinity*. NOAA Atlas NESDIS 3, US Gov. Printing Office.
- Maykut, G.A., Church, P.E., 1973. Radiation climate of Barrow, Alaska, 1962–1966. *J. Appl. Meteorol.* 12, 620–628.
- Melling, H., 2000. Exchanges of freshwater through the shallow straits of the North American Arctic. In: Lewis, E.L. (Ed.), *The Freshwater Budget of the Arctic Ocean*. Kluwer Academic Publishers, pp. 479–502.
- Mesinger, F., 1973. A method for construction of second-order accuracy difference schemes permitting no false two-grid-interval wave in the height field. *Tellus* 25, 444–457.
- Miller, J.R., Russell, G.L., 1995. Climate change and the Arctic hydrologic cycle as calculated by a global coupled atmosphere-ocean model. *Ann. Glaciol.* 21, 91–95.

- Pacanowski, R.C., 1995. MOM 2 Documentation (User's guide and reference manual). GFDL Ocean Tech. Rep., 3, Princeton University.
- Pardaens, A.K., Banks, H.T., Gregory, J.M., Rowntree, P.R., 2003. Freshwater transports in HadCM3. *Climate Dyn.* 21, 177–195.
- Parkinson, C.L., Washington, W.M., 1979. A large-scale numerical model of sea ice. *J. Geophys. Res.* 84, 311–337.
- Peterson, B.J., Holmes, R.M., McClelland, J.W., Vörösmarty, C.J., Lammers, R.B., Shiklomanov, A.I., Shiklomanov, I.A., Rahmstorf, S., 2002. Increasing river discharge to the Arctic Ocean. *Science* 298, 2171–2173.
- Plitkin, G.A., 1978. Inflow of surface waters into Siberian and Far Eastern seas and method of calculating it in individual years. *Water Res.* 5, 211–219.
- Prange, M., 2003. Einfluss arktischer Süßwasserquellen auf die Zirkulation im Nordmeer und im Nordatlantik in einem prognostischen Ozean-Meereis-Modell. Rep. Polar Mar. Res., 468, AWI, Bremerhaven, Germany.
- Prange, M., Lohmann, G., 2003. Effects of mid-Holocene river runoff on the Arctic ocean/sea-ice system: a numerical model study. *The Holocene* 13, 335–342.
- Prange, M., Lohmann, G., 2004. Variable freshwater input to the Arctic Ocean during the Holocene: Implications for large-scale ocean-sea ice dynamics as simulated by a circulation model. In: Fischer, H. et al. (Eds.), *The Climate in Historical Times: Towards a Synthesis of Holocene Proxy Data and Climate Models*. Springer-Verlag, Berlin, Heidelberg, New York, pp. 319–335.
- Prowse, T.D., Flegg, P.O., 2000. The magnitude of river flow to the Arctic Ocean: dependence on contributing area. *Hydrol. Process.* 14, 3185–3188.
- Rahmstorf, S., 1993. A fast and complete convection scheme for ocean models. *Ocean Model* (December), 9–11.
- Ranelli, P.H., Hibler, W.D., 1991. Seasonal Arctic sea-ice simulations with a prognostic ice-ocean model. *Ann. Glaciol.* 15, 45–53.
- Roach, A.T., Aagaard, K., Pease, C.H., Salo, S.A., Weingartner, T., Pavlov, V., Kulakov, M., 1995. Direct measurements of transport and water properties through the Bering Strait. *J. Geophys. Res.* 100, 18443–18457.
- Roeske, F., 2001. An atlas of surface fluxes based on the ECMWF re-analysis—A climatological dataset to force global ocean general circulation models. MPI Report, 323, MPI, Hamburg, Germany.
- Roulet, G., Madec, G., 2000. Salt conservation, free surface and varying volume: a new formulation for Ocean GCMs. *J. Geophys. Res.* 105, 23927–23942.
- Schlösser, P., Bayer, R., Bönisch, G., Cooper, L.W., Ekwurzel, B., Jenkins, W.J., Khatiwala, S., Pfirman, S., Smethie, W.M., 1999. Pathways and mean residence times of dissolved pollutants in the ocean derived from transient tracers and stable isotopes. *Sci. Tot. Environ.* 237/238, 15–30.
- Schmidt, G.A., Bitz, C.M., Mikolajewicz, U., Tremblay, L.-B., 2004. Ice-ocean boundary conditions for coupled models. *Ocean Model.* 7, 59–74.
- Semtner, A.J., 1976. A model for the thermodynamic growth of sea ice in numerical investigations of climate. *J. Phys. Oceanogr.* 6, 379–389.
- Semtner, A.J., 1984. The climatic response of the Arctic Ocean to Soviet river diversions. *Clim. Change* 6, 109–130.
- Semtner, A.J., 1987. A numerical study of sea ice and ocean circulation in the Arctic. *J. Phys. Oceanogr.* 17, 1077–1099.
- Simmons, H.L., Polyakov, I., 2004. Restoring and flux adjustment in simulating variability of an idealized ocean. *Geophys. Res. Lett.* 31, L16301. doi:10.1029/2004GL020197.
- Smolarkiewicz, P.K., 1983. A simple positive definite advection scheme with small implicit diffusion. *Mon. Weather Rev.* 111, 479–486.
- Steele, M., Thomas, D., Rothrock, D., Martin, S., 1996. A simple model study of the Arctic Ocean freshwater balance, 1979–1985. *J. Geophys. Res.* 101, 20833–20848.
- Steele, M., Boyd, T., 1998. Retreat of the cold halocline layer in the Arctic Ocean. *J. Geophys. Res.* 103, 10419–10435.
- Steele, M., Ermold, W., Häkkinen, S., Holland, D., Holloway, G., Karcher, M., Kauker, F., Maslowski, W., Steiner, N., Zhang, J., 2001a. Adrift in the Beaufort Gyre: a model intercomparison. *Geophys. Res. Lett.* 28, 2935–2938.
- Steele, M., Morley, R., Ermold, W., 2001b. PHC: a global ocean hydrography with a high quality Arctic Ocean. *J. Climate* 14, 2079–2087.
- Steiner, N., Holloway, G., Gerdes, R., Häkkinen, S., Holland, D., Karcher, M., Kauker, F., Maslowski, W., Proshutinsky, A., Steele, M., Zhang, J., 2004. Comparing modeled streamfunction, heat and freshwater content in the Arctic Ocean. *Ocean Model.* 6, 265–284.
- Tartinville, B., Campin, J.M., Fichefet, T., Goosse, H., 2001. Realistic representation of the surface freshwater flux in an ice-ocean general circulation model. *Ocean Model.* 3, 95–108.
- Vuglinsky, V.S., 1997. River water inflow to the Arctic Ocean—conditions of formation, time variability and forecasts. In: *Proceed. ACSYS Conf. Polar Proc. Global Clim.*, Rosario, Washington, pp. 275–276.
- Zalesak, S.T., 1979. Fully multidimensional flux-corrected transport algorithms for fluid. *J. Computat. Phys.* 31, 335–362.
- Zhang, J., Hibler, W.D., Steele, M., Rothrock, D.A., 1998. Arctic ice-ocean modeling with and without climate restoring. *J. Phys. Oceanogr.* 28, 191–217.
- Zhang, T., Etringer, A., Oelke, C., Frauenfeld, O., Barry, R.G., Gilichinsky, D., Serreze, M.C., Yang, D., Ye, H., Ling, F., Chudinova, S., submitted for publication. Inter-decadal variability in active-layer thickness over the Russian Arctic drainage basin. *J. Geophys. Res.*
- Zillman, J.W., 1972. A study of some aspects of the radiation and heat budgets of the southern hemisphere oceans. *Meteorol. Stud.*, 26, Bureau of Meteorol., Department of the Interior, Canberra.